DOI: 10.1002/adfm.200600448

Protein-Mediated Synthesis of Uniform Superparamagnetic Magnetite Nanocrystals**

By *Tanya Prozorov*, *Surya K. Mallapragada*,* *Balaji Narasimhan*,* *Lijun Wang*, *Pierre Palo*, *Marit Nilsen-Hamilton*, *Timothy J. Williams*, *Dennis A. Bazylinski*, *Ruslan Prozorov*, and *Paul C. Canfield*

Magnetite nanocrystals are synthesized in the presence of a recombinant Mms6 protein thought to be involved in the biomineralization of bacterial magnetite magnetosomes, the mammalian iron-storage protein, ferritin, and two proteins not known to bind iron, lipocalin (Lcn2) and bovine serum albumin (BSA). To mimic the conditions at which magnetite nanocrystals are formed in magnetotactic bacteria, magnetite synthesis is performed in a polymeric gel to slow down the diffusion rates of the reagents. Recombinant Mms6 facilitates formation of ca. 30 nm single-domain, uniform magnetite nanocrystals in solution, as verified by using transmission electron microscopy analysis and magnetization measurements. The nanocrystals formed in the presence of ferritin, Lcn2, and BSA, do not exhibit the uniform sizes and shapes observed for those produced in the presence of Mms6. Mms6-derived magnetite nanoparticles show the largest magnetization values above the blocking temperature, as well as the largest magnetic susceptibility compared to those of the nanomaterials synthesized with other proteins. The latter is indicative of a substantial effective magnetic moment per particle, which is consistent with the presence of magnetite with a well-defined crystalline structure. The combination of electron microscopy analysis and magnetic measurements confirms our hypothesis that Mms6 promotes the shape-selective formation of uniform superparamagnetic nanocrystals. This provides a unique bioinspired route for synthesis of uniform magnetite nanocrystals.

1. Introduction

There is increasing interest in using biomolecules to develop the next generation of advanced materials. Biomimetic synthetic routes offer the opportunity of controlling size, shape, crystal structure, orientation, and organization of nanoscale matter. In vitro use of mineralization proteins allows synthesis of a variety of nanostructured materials with unique properties.[1–5] Magnetic nanoparticles obtained via biomimetic routes can find applications as magnetic seals in motors, in spintronics, in magnetic inks, and in high-density magnetic memory devices.[2–4,6,7] The potential use of these nanoparticles in diagnostic medicine as contrast agents in magnetic resonance imaging (MRI) relies on the development of synthetic strategies that tailor particle uniformity, size, and dispersity.[7,8] The use of highly magnetic nanoparticle-containing contrast reagents can be advantageous because these nanoparticles are small enough to be localized in the desired region by applying local magnetic field gradients.[7–10] Another use of fine magnetic particles is in drug targeting and delivery. In the latter case, the use of uniform 30–40 nm magnetic nanoparticles provides high magnetic susceptibility values in the superparamagnetic regime.[7–10] The use of bacterial mineralization proteins to create magnetite nanoparticles in vitro offers the potential for facile synthesis of uniform magnetic nanocrystals with desirable morphologies and magnetic properties.

Magnetotactic bacteria form magnetite nanoparticles with various morphologies, including cuboctahedra, elongated hexahedra, or octahedra (appearing rectangular in projection in transmission electron microscopy (TEM), often referred to as pseudoprismatic and/or parallelepipedal), and tooth- or bullet shaped.[11–16] Magnetospirillum magneticum strain AMB-1 produces a chain of cuboctahedral magnetite nanocrystals each surrounded by a lipid bilayer membrane vesicle that appear to have several tightly bound membrane proteins.[17] Several proteins isolated from the magnetosome membranes of a number

[*] Prof. S. K. Mallapragada, Prof. B. Narasimhan, Dr. T. Prozorov
Department of Chemical and Biological Engineering
Iowa State University and Ames Laboratory
Ames IA 50011 (USA)
E-mail: suryakm@iastate.edu; nbalaji@iastate.edu
L. Wang, P. Palo, Prof. M. Nilsen-Hamilton
Dr. T. J. Williams, Prof. D. A. Bazylinski
Department of Biochemistry, Biophysics and Molecular Biology
Iowa State University
Ames IA 50011 (USA)
Dr. R. Prozorov, Prof. P. C. Canfield
Department of Physics and Astronomy
Iowa State University and Ames Laboratory
Ames IA 50011 (USA)

[**] We thank Lee Bendickson and Yinghua Liu for providing Lcn2 and His-Lcn2. This research was supported by the U.S. Department of Energy grant W-7405-ENG-82. D.A.B. and T.J.W were partially supported by a U.S. National Science Foundation grant EAR-0311950. R.P. was partially supported by U.S. National Science Foundation Career grant DMR-0603841. XRD measurements were carried out in the Center for Microanalysis of Materials, University of Illinois, which is partially supported by the U.S. Department of Energy under grant DEFG02-91-ER45439. Supporting Information is available online from Wiley InterScience or from the author.

of magnetotactic bacterial species appear to be specifically localized in the magnetosome vesicle membranes.[17–20] Some of these proteins have hydrophobic N termini and hydrophilic C termini containing a large number of carboxylic and hydroxyl side chains that are known to bind iron ions.[17] One such protein, Mms6, was found by Arakaki et al.[17] to facilitate in-vitro formation of cuboidal magnetite particles resembling those found in some magnetotactic bacteria. Despite the successful in vitro synthesis of nanoparticles with shapes and sizes resembling those found in Magnetospirillum magneticum strain AMB-1, it is unclear whether shape-selective formation of nanocrystals was solely due to the presence of Mms6.[17] In addition, magnetization and structural characterization of the magnetite materials prepared by Mms6 templating are lacking in this report.[17] Furthermore, owing to their synthesis in aqueous solutions with consequent rapid nanocrystal formation, the reported nanoparticles lacked uniformity. In this paper, we present a new bioinspired synthetic route to prepare uniform nanoparticles and important magnetic and structural characterization of magnetite nanocrystals prepared by using protein templating.

To elucidate whether the formation of the uniform ca. 30 nm magnetite nanoparticles was specifically due to Mms6, we compared several proteins for their ability to promote the growth of shape-specific magnetic iron oxide nanocrystals. The ability of Mms6 to stimulate formation of magnetite nanocrystals was compared to that of three other control proteins that bind iron in different ways: ferritin that forms a cage around the iron to create 3–5 nm particles;[21–25] lipocalin (Lcn2; also called uterocalin, 24p3, and siderocalin) that binds siderophore-chelated iron[26] and was produced as a His-tagged recombinant protein (as was Mms6); and bovine serum albumin (BSA) that binds iron nonspecifically. We hypothesize that the viscosity of the reaction media is an important factor in the formation of uniform magnetite nanocrystals.[27–29] To this end, the nanoparticles were formed in aqueous solutions and in the presence of viscous aqueous Pluronic F127 gels[28,29] to better mimic the synthetic environment within an organism.

2. Results and Discussion

We compared the ability of Mms6 to promote the formation of magnetite nanocrystals with that of three other proteins, each known to bind iron differently, as discussed above. We also included magnetite nanoparticles obtained via protein-free co-precipitation synthesis as a negative control. Figure 1 shows TEM images obtained from protein-assisted co-precipitation in the viscous[27–29] media. The protein-free magnetite nanoparticles (Fig. 1A) showed significant size and shape dispersity. In contrast, Mms6 appears to facilitate the formation of uniform nanoparticles of magnetite in solution with defined morphology, with a mean crystallite size of ca. 30 nm, as seen in Figure 1B. In Figure 1C, the nanoparticles synthesized in the presence of ferritin appear to be enveloped in a protein matrix. Here the ferritin-derived material contains large numbers of ill-defined encapsulated iron oxide nanoparticles of significantly smaller size than the particles synthesized in the presence of Mms6 (Fig. 1B). Similarly, a sample of magnetite prepared in the presence of His-Lcn2 (Fig. 1D) showed nanoparticles of markedly smaller size lacking the defined particle morphology.

As the His-Lcn2-derived nanoparticles lacked the same shape as the Mms6-promoted particles, this indicated that although it binds iron, the His-tag present in both recombinant Mms6 and His-Lcn2 is unlikely to direct the formation of robust isomorphic nanocrystals. Finally, the magnetite crystallites obtained in the presence of BSA (Fig. 1E) were polydisperse in both size and shape and did not exhibit the larger particles with defined morphology. None of the control proteins produced nanoparticles with similar morphology to that pro-

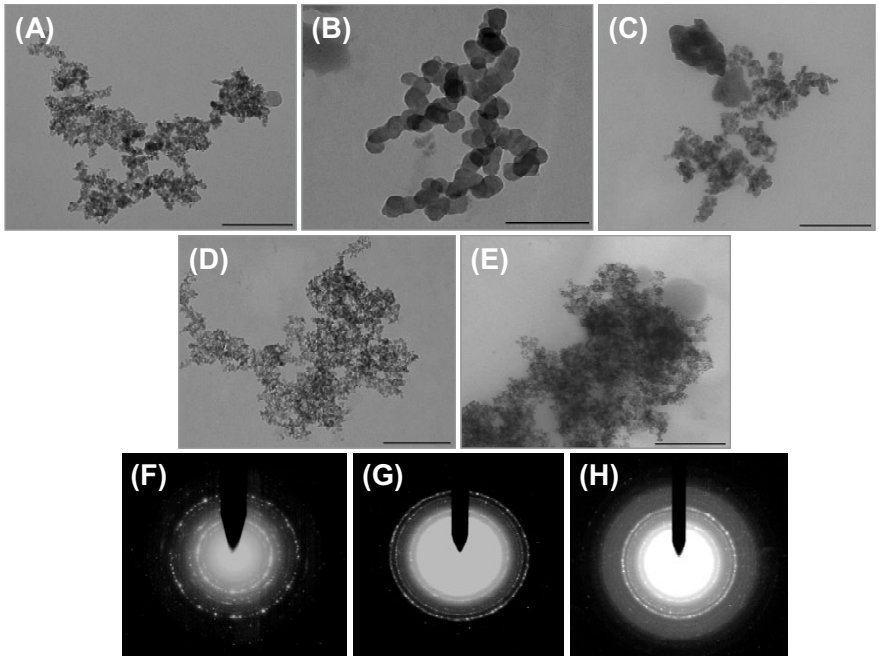

Figure 1. TEM images of magnetite nanoparticles obtained by co-precipitation of $FeCl_2$ and $FeCl_3$: A) without protein, B) with Mms6, C) with ferritin (Note that ca 5 nm iron oxide nanoparticles seen as darker small dots appear embedded in surrounding globular bodies, most likely protein), D) with Lnc2, and E) with BSA. F) Selected-area electron diffraction pattern of Mms6-derived magnetite cluster with random orientation showing varying intensities of the diffraction rings; G) selected-area electron diffraction pattern of Lcn2-derived magnetite cluster with random orientation, showing weaker intensity and a larger number of the electron diffraction peaks; and H) the selected-area electron diffraction pattern from ferritin-derived magnetite nanoparticles. Here the individual electron diffraction peaks overlap and form electron diffraction rings, which is consistent with the presence of a large number of small and randomly oriented nanoparticles. Scale bars: 200 nm.

ADVANCED FUNCTIONAL MATERIALS

duced in the presence of Mms6. Selected-area electron diffraction patterns for Mms6-derived magnetite (Fig. 1F) and His-Lcn2-derived magnetite (Fig. 1G) are consistent with the size and morphology of nanoparticles observed in each case using TEM. The electron diffraction pattern of the Mms6-derived magnetite nanocrystals with a random orientation exhibited several strong and easily distinguishable diffraction peaks, as shown in Figure 1F. This is consistent with the presence of larger particles with a well-established crystalline structure. On the other hand, the electron diffraction pattern of the His-Lcn2-derived magnetite showed peaks with weaker intensities (Fig. 1G). Here, the diffraction peaks from the individual nanocrystals are difficult to distinguish, which is consistent with the presence of a significant number of randomly oriented smaller nanoparticles. In the electron diffraction pattern obtained from the ferritin-derived magnetite, individual electron diffraction peaks are hard to tell apart, and these peaks overlap to form the diffraction rings. Such a display is consistent with the presence of a large number of small and randomly oriented nanoparticles.

The powder X-ray diffraction (XRD) patterns of the synthesized magnetic materials displayed peak line positions and relative intensities consistent with the crystal structure of magnetite. However, owing to similarities in the magnetite and maghemite diffraction patterns, XRD cannot be used to completely refute the presence of fully oxidized iron oxide, maghemite. Figure 2 shows an X-ray powder diffraction pattern of the Mms6-derived sample, identified as magnetite. Mms6-derived magnetite XRD pattern ((Cu Kα), *d*-spacing: 4.706, 4.571, 3.780, 2.925, 2.05 2.404, 2.081, 1.701, 1.601, 1.473, 1.318, 1.274, 1.263, 1.200, 1.114 Å. The asterisk denotes an impurity peak, most likely bernalite ($Fe(OH)_3(H_2O)_{0.25}$).

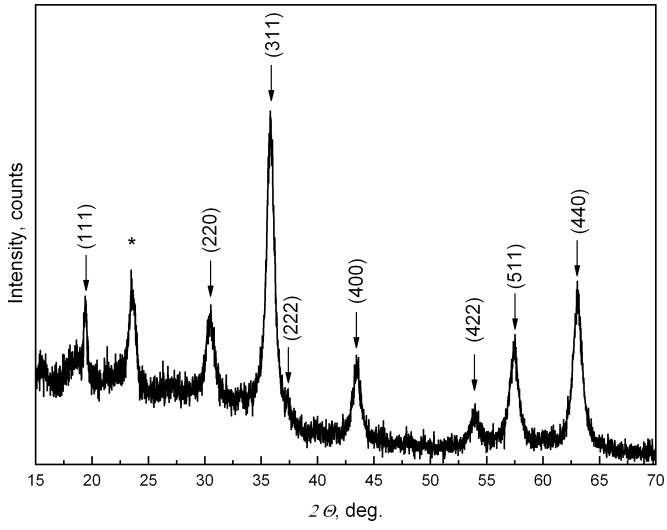

Figure 2. X-ray powder diffraction pattern of the Mms6-derived precipitated magnetite after washing in water and drying in vacuum overnight. The asterisk indicates an impurity peak.

The magnetic response of nanoscale materials is determined by the particle size, morphology, structure, and anisotropy as well as interparticle interactions (usually dipole–dipole), especially at low temperatures. As a result, comparative characterization of superparamagnetic suspensions is complex.[30,31] Some understanding of the properties of individual particles can be achieved by performing measurements of magnetization as a function of temperature, magnetic field, and time. A detailed study of the magnetic properties of nanoparticles described in this paper will be reported elsewhere. Here, we only summarize the results necessary to compare the properties of particles created in the presence of Mms6 and other proteins.

The superparamagnetic nature of the nanoparticles was established by comparing zero-field cooling (ZFC) and field-cooling (FC) curves. The characteristic blocking temperature determined from the maximum of the ZFC curve in a 500 Oe (1 Oe = 1000/4π A m^{-1}) applied field was between 30 and 50 K for all samples studied, which is in agreement with previous studies.[30,31]

Figure 3 shows magnetization loops for different samples, normalized to the saturation value obtained at $H = 5$ Tesla. The important characteristics to consider here are the width of the hysteresis loops and steepness of the $M(H)$ curve at low fields. The former is indicative of the collective barrier strength in the blocked state; the latter is mostly related to the effective mag-

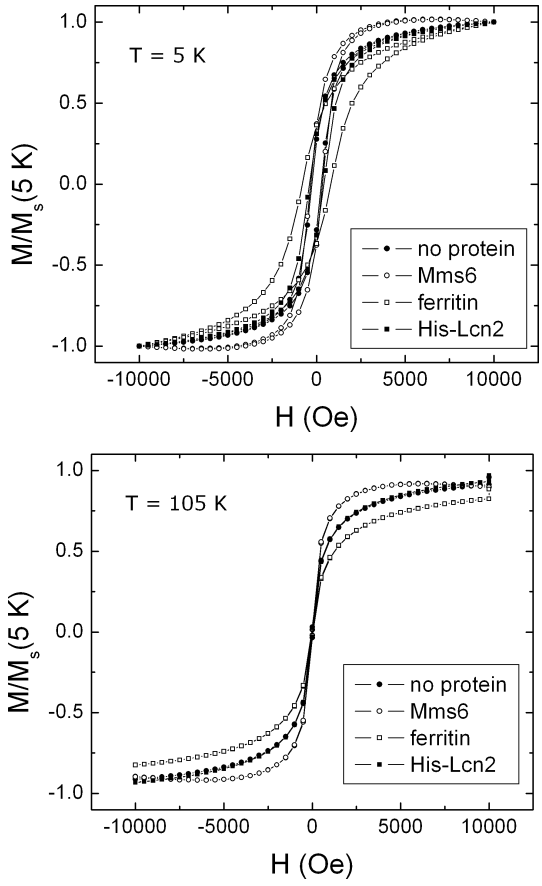

Figure 3. Normalized magnetization $M(H)$ loops for different samples as described in the text. Upper frame: at $T = 5$ K (below blocking temperature); lower frame: at $T = 105$ K (above blocking temperature).

netic moment of individual nanoparticles. Clearly, the largest hysteresis below the blocking temperature was observed for the ferritin-derived sample, which is consistent with a strongly interacting assembly of small particles. However, the magnetization curve in the material obtained with Mms6 climbed to saturation in smaller fields, which is indicative of a higher magnetic moment per particle. Its hysteretic behavior is similar to that of the protein-free and the His-Lcn2-derived samples. At temperatures well above the blocking temperature (T_B) (lower frame in Fig. 3), hysteresis is negligible in all samples and curves follow the Langevin function, which describes the superparamagnetic state above T_B. Protein-free and His-Lcn2-derived materials exhibited almost identical behavior, indicating no noticeable effect of His-Lcn2.

By fitting the data to the Langevin function we can estimate the parameter $p\mu_B/k_BT$, where p is the number of Bohr magnetons (μ_B), per particle. These estimates, however, do not account for possible contributions of surface spin canting and magnetocrystalline anisotropy. Therefore, this procedure is the most reliable for the smallest poorly crystalline nanoparticles, such as those produced with ferritin. In this case, p is determined to be ca. 4×10^3 μ_B. Assuming the literature data of $4\mu_B$ per unit of Fe_3O_4,[32] we obtain a particle size of 5 nm, in good agreement with direct TEM observations. Protein-free magnetite nanoparticles and Mms6-derived nanoparticles are larger and therefore should have larger magnetic moment per particle.

When the magnetic field was turned off at 5 K after completing the field cooling–cooling measurements, there was remanent (trapped) nonequilibrium magnetization determined by both the collective barrier and individual coercivities of the nanoparticles. Below T_B, remanent magnetization was mostly determined by the collective barrier, but above T_B, only individual coercivities contribute. The corresponding coercivity was also large as explained by the Stoner–Wohlfarth model.[33] The individual particle coercivity was significantly enhanced in crystalline and well-shaped particles. Enhanced crystal anisotropy and shape anisotropy as well as reduced surface spin canting contributed. In this way, the temperature dependence of remanent magnetization can be used to compare amorphous (ill-shaped) and crystalline (well-shaped) particles.

Figure 4 shows annealing of the remanent magnetic moment for characteristic samples from each group. The particles prepared in the absence of protein and those prepared with ferritin showed similar behavior. The amorphous-like nanoparticles produced in the presence of ferritin were the smallest, which is consistent with previous reports.[1,5,23,34–37] The magnetite particles formed in the presence of Mms6 showed distinctly different behavior, with much larger remanence lasting well above the blocking temperature. Such behavior is indicative of a larger magnetic moment per particle and consistent with the presence of magnetite with a well-defined crystalline structure.[38,39]

Overall, the magnetic measurements were fully consistent with the electron microscopy observations. The nanoparticles showed superparamagnetic behavior, in good agreement with the observed shapes and sizes. Mms6-derived nanoparticles

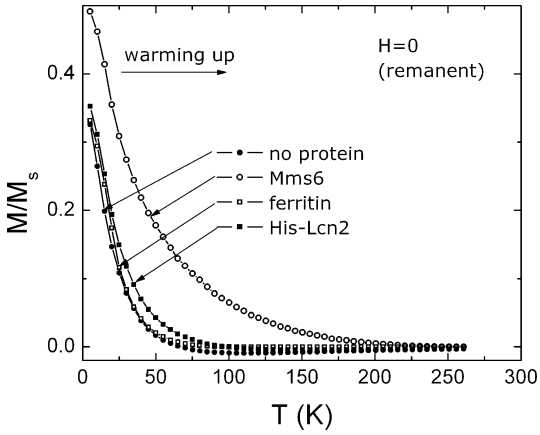

Figure 4. Annealing of the remanent magnetization obtained after the magnetic field is removed after cooling. Mms6-derived magnetite clearly shows the highest irreversibility—up to > 200 K.

exhibited a higher blocking temperature and magnetic susceptibility, which are consistent with the presence of larger magnetite nanocrystals with a well-defined crystalline structure. The magnetite samples produced with recombinant Mms6 protein showed the largest magnetic susceptibility and remanence. Both behaviors are consistent with our initial hypothesis that Mms6 has the unique ability to promote the formation of ca. 30 nm uniform isomorphic superparamagnetic magnetite nanocrystals. Under identical synthetic conditions, ferritin stimulated the formation of encapsulated poorly crystalline iron oxide nanoparticles of significantly smaller size. The difference in morphology and size of the formed nanoparticles can be preliminarily interpreted in terms of differences in protein sizes, structures, and iron binding mechanisms. The most plausible explanation involves the relatively large size of the ferritin molecule (ca. 24 kDa)[23,40] compared to the Mms6 molecule (ca. 6 kDa), thereby providing a larger number of iron binding sides serving as nucleation sites in the crystal-growth process. Thus, the ferritin-derived material contains a larger number of smaller particles.[23,40] The properties of the novel Mms6 protein remain largely unexplored; however, the comprehensive study of structural stability and the properties and of Mms6 protein is a subject of active research. All the remaining magnetite samples consisted of ill-defined, amorphous-like particles, which indicated that there was no apparent influence of the His-Lcn2 or BSA on the particle morphology.

3. Conclusions

By using various proteins in viscous reaction media, we have successfully controlled the structure, morphology, and average size of the resulting magnetite nanocrystals, and the magnetic interparticle interactions. Mms6 promoted the formation of uniform isomorphic magnetite nanocrystals, which was not achieved by any of the three control proteins, each binding iron in a different way. TEM revealed a distinct morphology of the

magnetite sample synthesized in the presence of Mms6 which was consistent with magnetic properties. Comprehensive analysis of the nanostructured magnetite samples obtained via protein-mediated synthesis confirms the hypothesis that the Mms6 serves as a template for the formation of uniform, isomorphic, superparamagnetic nanocrystals. The role of this mineralization protein in magnetite synthesis by co-precipitation is further emphasized in comparison to magnetite synthesis in the presence of ferritin. The use of biomineralization protein provides a unique bioinspired route for the synthesis of ca. 30 nm isomorphic uniform superparamagnetic nanocrystals.

4. Experimental

Materials and Reagents: All solutions were degassed and sparged with argon prior to their use. Pluronic F127 NF Prill Poloxamer 407 (BASF) was dissolved in toluene, recrystallized from cold hexane, and dried overnight in vacuo at room temperature. $FeCl_3 \cdot 6H_2O$ (Aldrich) and $FeCl_2 \cdot 4H_2O$ (Aldrich) were transferred to a reaction flask and dissolved in water to form a solution with a 1:2 molar ratio of ferrous to ferric ions (i.e., 0.66 M $FeCl_3$ and 0.33 M $FeCl_2$ solutions, respectively). Ferritin (CalBiochem), BSA (Sigma), and other proteins used in the study were dialyzed against the identical buffer (20 mM trisphosphate, 20 % glycerol, 100 mM KCl, pH 7.5).

Expression and Purification of His-Lcn2 and Lcn2: The bacterial expression vector, pTrcHisUtc2, encoding Lcn2 with an N-terminal histidine (His) tag (His-Lcn2) and an enterokinase site C terminal to the His-tag was constructed as described by Playford et al. [41]. The protein was expressed in *Escherichia coli* stimulated by isopropyl β-D-1-thiogalactopyranoside. For its purification, His-Lcn2 was captured from the bacterial cell lysate using nickel chelate chromatography (Ni-NTA; Qiagen). The resin was first washed with buffer 1 (50 mM NaPi, 300 mM NaCl, pH 6.0), then His-Lcn2 was eluted with buffer 2 (50 mM NaPi, 300 mM NaCl, pH 4.5). The amount of protein in each sample was determined by the Bradford protein assay [42]. The purified protein was evaluated for its purity by using gel electrophoresis (Fig. 5C) and western blot using anti-Lcn2 antibodies (not shown). To prepare Lcn2, 3 mL of His-Lcn2 (0.3 mg mL^{-1}) was incubated with 30 Units mL^{-1} of recombinant enterokinase (EK, Novagen) in 84 mM NaCl, 2.2 mM $CaCl_2$, 22 mM Tris-HCl, 1.2 mM $NaKPO_4$, 5 % Glycerol, pH 7.4. The protein was incubated at 30 °C for 20 h then passed through an EK capture column (Novagen) to remove the EK. The Lcn2 was separated from the His-tag and His-Lcn2 by passing the remaining protein through the Ni-NTA column and collecting the flow-through.

Cloning and Expression of the Recombinant Mature Mms6 Protein: Genomic DNA was obtained from Magnetospirillum magneticum strain AMB-1. The DNA was amplified using primers that are complementary to internal sites on the Mms6 gene coding region. The genomic DNA was amplified using primers that are complementary to internal sites on the Mms6 gene coding region. The primers were designed to amplify the region of the gene corresponding to the mature Mms6 protein [17] (Fig. 5A). The polymerase chain reaction (PCR) amplicon was cloned into the plasmid pTrcHis TOPO such that the Mms6 sequence is in frame with an N-terminal polyhistidine tag (Invitrogen). This cloned expression vector was used to prepare recombinant mature Mms6 protein. Cells of *Escherichia coli* transformed by Mms6 expression vectors were used to produce His-tagged Mms6. Some of the expressed Mms6 was found in the soluble fraction of the bacterial lysates. However, a large fraction of the expressed Mms6 was insoluble and present in inclusion bodies. The inclusion body was dissolved in 8 M urea, Mms6 retrieved by way of the His-tag as described for His-Lcn2 and refolded by sequential dialysis against increasingly lower concentrations of urea in 20 mM Tris, 500 mM KCl, 20 % glycerol, 0.2 mM phenylmethanesulfonyl fluoride, pH 7.5. The amount of protein in each sample was determined by the Bradford protein assay [42]. The purified proteins were evaluated for their purity by using gel electrophoresis and western blot using anti-His-tag antibodies (Fig. 1B).

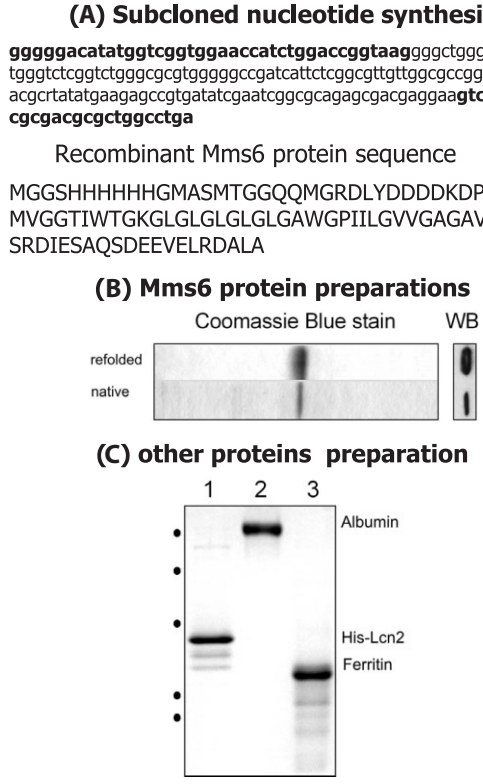

Figure 5. Mms6 and other proteins used in this study: A) the nucleotide sequence that was cloned from the Magnetospirillum magneticum genome including the primers used for PCR, which are in bold and the sequence of the recombinant His-tagged Mms6 protein; B) Mms6 protein preparations were resolved by sodium dodecyl sulfate polyacrylamide gel electrophoresis (SDS PAGE) and either stained for protein with Coomassie blue or blotted to nitrocellulose and stained with antibody to the His-tag (Amersham Biosciences) following a Western blot protocol; C) other protein preparations used in this study were resolved by SDS PAGE: 1) His-Lcn2, 2) BSA, 3) ferritin. The dots on the left are the positions of the molecular mass standard proteins (S) that were from top to bottom 68, 45, 30, 18, and 12 kDa.

Iron Binding Analysis: His-Mms6, ferritin, His-Lcn2, Lcn2, and BSA were incubated in separate tubes for 1 h each at 0.67 μM and with 10 μM Fe^{55}, 0.15 M NaCl, 10 mM KCl, 2 % glycerol, 0.022 M Tris-HCl, pH 7.0 (at 23 °C) under argon. The samples were then filtered through 0.45 μM nitrocellulose membranes (Millipore, Cat#: HAWP 02500) that had been prewashed with wash buffer (0.02 M Tris-HCl, 0.15 M NaCl, pH 7.0 at 23 °C). The membranes were washed with two consecutive 5 mL aliquots of wash buffer then removed and counted using Scintiverse biodegradable liquid scintillation cocktail, Fisher Scientific, Cat#:SX18-X scintillant and a Packard model 1600 TR liquid scintillation analyzer. Buffers used for this analysis of binding capability were degassed and sparged with argon before use. The ability of the four proteins to bind iron was tested using a filter assay and Fe^{55}. As shown in Figure 6, Mms6 binds slightly less iron than ferritin on a molar basis. However, some of this iron binding by Mms6 is likely to be due to the His-tag as demonstrated by the comparison of the iron binding ability of His-Lcn2 and Lcn2. Once the His-tag is removed, Lcn2 has almost the same iron binding ability as BSA. Similar results were found at 1, 10, and 100 μM iron. It is worth noting, however, that His-tagged Mms6 bound more iron than His-Lcn2.

Protein-Mediated Magnetite Synthesis: Synthesis of magnetite nanoparticles was carried out via co-precipitation of $FeCl_2$ and $FeCl_3$ from

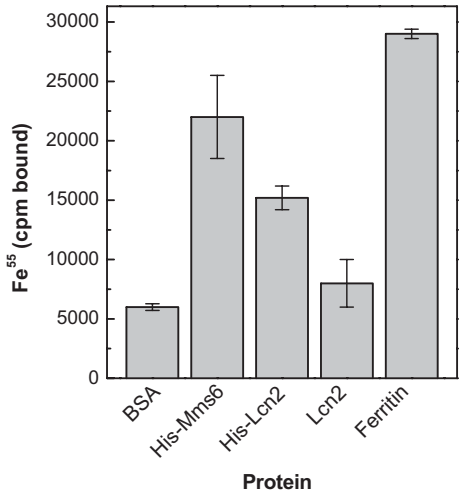

Figure 6. Iron binding abilities of various proteins. The proteins used in this study were tested for their ability to bind iron as described in the Experimental section. The data is the average of three experiments. In each experiment each protein was tested at 0.67 μM in triplicate and the average cpm of Fe^{55} bound by each protein is represented by a bar above the protein name with the standard deviations represented as error bars. The iron concentration was 10 μM.

aqueous solutions in the presence of one of several proteins, including Mms6, ferritin, His-Lcn2, or BSA. Initially, magnetite synthesis was carried out in degassed water. The synthesis in the presence of Mms6 yielded magnetite nanometer-sized crystals with a wide size dispersity, lacking specific crystal morphology. In order to slow the diffusion rates of the reagents to better imitate the conditions under which magnetite nanocrystals are formed in magnetotactic bacteria, F-127 Pluronic polymeric aqueous gel was introduced into the reaction mixture. F-127 Pluronic aqueous solutions exhibit reverse temperature gelation, thus forming viscous gels at room temperature [27–29]. Viscosity of 18–30 wt % Pluronic solutions changes from ca. 100 cP (1 cP = 0.001 Pa s) at 4 °C to significantly higher values at room temperature [29], whereas the viscosity of distilled water in the same temperature range remains at ca. 1 cP [32]. In a typical experiment, protein solutions containing 4 μg of Mms6, ferritin, His-Lcn2, or BSA, were added to 100 μL of cooled 20 wt % F-127 Pluronic aqueous solution, placed in a 10 mL roundbottomed flask, degassed and sparged with argon. To this solution, several microliters of room-temperature buffer solution degassed and sparged with argon were added to maintain equal volume and an equal protein-to-buffer ratio in each reaction vessel. Each flask was then charged with 100 μL of 0.66 M $FeCl_3$ and 0.33 M $FeCl_2$ solution, and a drop of 0.0016 M of HCl, vigorously stirred, and sparged with argon for 1 min. To ensure that F-127 Pluronic aqueous gel was in a liquid phase in order to achieve uniform mixing, the reaction flasks were incubated at 4 °C for 15 min prior to the reaction. The resulting solution was then brought to room temperature, and titrated slowly with the room-temperature 0.1 M NaOH solution under constant argon flow. As the titration progressed, the initially pale yellow solution gradually changed to brownish-yellow, then dark green, and finally to black. Nanoparticles were allowed to grow and precipitate at room temperature at pH 7 in the sealed flask for 5 days, after which the precipitated nanoparticles were concentrated at the bottom of the flask with a magnet, thus ensuring collection of the magnetic fraction of the precipitate. An aliquot of magnetically separated concentrated suspension was taken for magnetic measurements. The remaining precipitate was washed with a small amount of degassed water (2 × 5 mL) under Ar flow, and vacuum dried overnight at room temperature.

Materials Characterization: Particle size and morphology of synthesized magnetite materials were examined by using a JEOL 1200EX scanning TEM at an accelerating voltage of 80 kV. Diluted magnetite suspensions were placed on carbon-coated copper grids and dried at room temperature. Electron diffraction patterns were obtained by using a Philips CM30 transmission electron microscope at an accelerating voltage of 300 kV, unless stated otherwise.

Powder XRD analysis was performed by using a Rigaku D/MAX diffractometer (45 kV, 20 mA) with graphite-monochromatized Cu Kα radiation ($\lambda = 1.54178$ Å). Diffractograms were collected with a 2θ–θ step-scan mode with the scan speed maintained at 2 deg min^{-1}, with 0.02 deg. step interval.

Magnetization measurements were carried out by using a quantum design superconducting quantum interference device (SQUID) 5T magnetic properties measurement system (MPMS). Freshly synthesized magnetite suspension was injected into a polycarbonate capsule and immediately cooled below the freezing temperature of the liquid. To allow comparison between differently synthesized nanoparticles, magnetization loops measurements, $M(H)$, at different temperatures ranging from 5 to 280 K were performed. In addition, temperature scans, $M(T)$, were performed following different protocols. For example, comparison of zero-field cooled and field-cooling magnetization clearly indicated the superparamagnetic (monodomain) nature of the nanoparticles. In another experiment, the magnetic field was turned off after cooling in a high magnetic field and the sample was slowly warmed up to measure the so-called "remanent magnetization".

Received: May 24, 2006
Revised: July 18, 2006
Published online: February 13, 2007

[1] M. Allen, M. Klem, K. Gilmore, Y. Idzerda, M. Young, T. Douglas, *Polym. Mater. Sci. Eng.* **2004**, *90*, 315.
[2] J. D. Birchall, *Mater. Res. Soc. Symp. Proc.* **1993**, *286*, 297.
[3] T. Douglas, M. Allen, M. Klem, K. Gilmore, Y. Idzerda, M. Young, *Polym. Mater. Sci. Eng.* **2004**, *90*.
[4] M. T. Klem, M. Young, T. Douglas, *Mater. Today (Oxford, U.K.)* **2005**, *8*, 28.
[5] C. W. Lawton, C. S. Shields, *Mater. Res. Soc. Symp. Proc.* **1993**, *292*, 107.
[6] H. Ai, C. Flask, B. Weinberg, X. Shuai, M. D. Pagel, D. Farrell, J. Duerk, J. Gao, *Adv. Mater.* **2005**, *17*, 1949.
[7] P. Tartaj, M. del Puerto Morales, S. Veintemillas-Verdaguer, T. Gonzalez-Carreno, C. J. Serna, *J. Phys. D: Appl. Phys.* **2003**, *36*, R182.
[8] Q. A. Pankhurst, J. Connolly, S. K. Jones, J. Dobson, *J. Phys. D: Appl. Phys.* **2003**, *36*, R167.
[9] A. Ditsch, P. E. Laibinis, D. I. C. Wang, T. A. Hatton, *Langmuir* **2005**, *21*, 6006.
[10] G. D. Moeser, W. H. Green, P. E. Laibinis, P. Linse, T. A. Hatton, *Langmuir* **2004**, *20*, 5223.
[11] D. A. Bazylinski, *Int. Microbiol.* **1999**, *2*, 71.
[12] D. A. Bazylinski, R. B. Frankel, *Nat. Rev. Microbiol.* **2004**, *2*, 217.
[13] R. P. Blakemore, *Annu. Rev. Microbiol.* **1982**, *36*, 217.
[14] B. Devouard, M. Posfai, X. Hua, D. A. Bazylinsi, R. B. Frankel, P. R. Buseck, *Am. Mineral.* **1998**, *83*, 1387.
[15] M. R. McCartney, U. Lins, M. Farina, P. R. Buseck, R. B. Frankel, *Eur. J. Mineral.* **2001**, *13*, 685.
[16] A. P. Taylor, J. C. Barry, *J. Microsc.* **2004**, *213*, 180.
[17] A. Arakaki, J. Webb, T. Matsunaga, *J. Biol. Chem.* **2003**, *278*, 8745.
[18] T. Matsunaga, H. Takeyama, *Supramol. Sci.* **1998**, *5*, 391.
[19] U. Lins, M. Farina, B. Kachar, *Microbiol. Res.* **2003**, *158*, 317.
[20] A. Scheffel, M. Gruska, D. Faivre, A. Linaroudis, J. M. Plitzko, D. Schueler, *Nature* **2005**, *440*, 110.
[21] R. B. Frankel, *Francis Bitter Natl. Magn. Lab.*, Massachusetts Inst. Technol., Cambridge, MA **1988**, p. 21.
[22] S. A. Malone, A. Lewin, M. A. Kilic, D. A. Svistunenko, C. E. Cooper, M. T. Wilson, N. E. Le Brun, S. Spiro, G. R. Moore, *J. Am. Chem. Soc.* **2004**, *126*, 496.
[23] E. C. Theil, *J. Nutr.* **2003**, *133*, 1549S.
[24] S. Clemens, C. Simm, T. Maier, *Biopolymers* **2003**, *8*, 255.

ADVANCED FUNCTIONAL MATERIALS

[25] D. P. E. Dickson, S. A. Walton, S. Mann, K. Wong, *Nanostruct. Mater.* **1997**, *9*, 595.
[26] D. H. Goetz, M. A. Hoimes, N. Borregaard, M. E. Bluhm, K. N. Raymond, R. K. Strong, *Mol. Cell* **2002**, *10*, 1033.
[27] K.-i. Kurumada, B. H. Robinson, in *Progress in Colloid and Polymer Science*, Vol. 123 (Eds: M. da Graca Miguel, H. D. Burrows), Springer, Berlin **2004**, p. 12.
[28] K. Mortensen, *J. Phys.: Condens. Matter* **1996**, *8*, A103.
[29] R. L. Rill, B. R. Locke, Y. Liu, D. H. van Winkle, *Proc. Natl. Acad. Sci. USA* **1998**, *95*, 1534.
[30] R. Prozorov, Y. Yeshurun, T. Prozorov, A. Gedanken, *Phys. Rev. B: Condens. Matter Mater. Phys.* **1999**, *59*, 6956.
[31] R. Prozorov, T. Prozorov, *J. Magn. Magn. Mater.* **2004**, *281*, 312.
[32] D. R. Lide, *Handbook of Chemistry and Physics*, 82nd ed., CRC Press, Boca Raton **2002**, p. 2500.
[33] E. C. Stoner, E. P. Wohlfarth, *Philos. Trans. R. Soc. London Ser. A* **1948**, *240*, 599.
[34] S. Bailey, R. W. Evans, R. C. Garratt, B. Gorinsky, S. Hasnain, C. Horsburgh, H. Jhoti, P. F. Lindley, A. Mydin, R. Sarra, J. L. Watson, *Biochemistry* **1988**, *27*, 5804.
[35] Q. A. Pankhurst, P. Allen, N. S. Cohen, I. Colbeck, G. D. Forster, D. Jeffery, *J. Aerosol Sci.* **1998**, *29*, S913.
[36] A. Sinha, S. Nayar, G. V. S. Murthy, P. A. Joy, V. Rao, P. Ramachandrarao, *J. Mater. Res.* **2003**, *18*, 1309.
[37] I. Yamashita, *Thin Solid Films* **2001**, *393*, 12.
[38] T. Polyakova, V. Zablotskii, *J. Magn. Magn. Mater.* **2005**, *293*, 365.
[39] R. Hergt, R. Hiergeist, M. Zeisberger, D. Schueler, U. Heyen, I. Hilger, W. A. Kaiser, *J. Magn. Magn. Mater.* **2005**, *293*, 80.
[40] X. Liu, E. C. Theil, *Proc. Natl. Acad. Sci. USA* **2004**, *101*, 8557.
[41] R. Playford, A. Belo, R. Poulsom, A. Fitzgerald, K. Harris, I. Pawluczyk, J. Ryon, T. Derbi, M. Nilsen-Hamilton, T. Marchbank, *Gastroenterology*, in press.
[42] M. M. Bradford, *Anal. Biochem.* **1976**, *72*, 248.